Enhanced Raman scattering by molecules adsorbed at the surface of colloidal spheroids

D. -S. Wang and M. Kerker
Clarkson College of Technology, Potsdam, New York 13676
(Received 26 February 1981)

Equations are derived and calculations are presented for the electrodynamic mechanism of enhanced Raman scattering by molecules at the surface of prolate and oblate spheroids in the small-particle limit. The molecules may be arbitrarily distributed; the particles may be arbitrarily oriented. Calculations are presented for a monolayer distributed over randomly oriented spheroids. The effects of particle shape are considered for Ag, Au, and Cu hydrosols. The peak enhancement moves to longer wavelengths, and in the case of Au and Cu the magnitude of the enhancement increases strikingly as the eccentricity increases. The relation between the dependence of the Raman enhancement upon excitation wavelength and the extinction spectra is discussed, including the precariousness of extrapolating such relations beyond the small-particle limit.

I. INTRODUCTION

The prediction by Moskovits that surface-enhanced Raman scattering (SERS) observed at certain roughened metal electrodes might also occur with molecules adsorbed onto colloidal particles[1] was first verified by Creighton, Blatchford, and Albrecht utilizing silver and gold hydrosols.[2] There have since been a number of other reports of SERS on colloidal hydrosols,[3] including one by us for which the measured enhancement of citrate adsorbed on colloidal silver increased monotonically from less than 3×10^3 for excitation wavelength 350.7 nm up to 6×10^5 for 647.1 nm.[4]

The study of dilute colloidal hydrosols has an advantage in that the critical sensitivity of the enhancement to the scale of "roughness" of a macroscopic surface becomes transformed in the case of colloidal particles to a dependence of the enhancement upon particle size and shape—quantities which can be observed and which can be described deterministically.

Indeed, we have formulated a general electrodynamic theory of SERS by molecules adsorbed at the surface of spherical particles.[5] A molecule is treated as a classical electric dipole located at an arbitrary position $\vec{r}'$ outside of an isotropic homogeneous sphere, including positions on the surface. There are no restrictions on the location or orientation of the molecule, nor on the radius of the sphere or its relative complex refractive index. When a plane electromagnetic wave of circular frequency ω_0 is incident, the dipole will radiate at the Raman frequency ω with dipole moment

$$\vec{p}(\vec{r}',\omega) = \underline{\alpha}_m \cdot \vec{E}_p(\vec{r}',\omega_0) \quad , \tag{1}$$

where $\underline{\alpha}$ is the molecular Raman polarizability, and the primary field $\vec{E}_p(\vec{r}',\omega_0)$ at $\vec{r}'$ and frequency ω_0 denotes the incident field $\vec{E}_i(\vec{r}',\omega_0)$ plus the elastically scattered field $\vec{E}_{\rm LM}(\vec{r}',\omega_0)$ as calculated by the Lorenz-Mie theory[6]

$$E_p(\vec{r}',\omega_0) = E_i(\vec{r}',\omega_0) + E_{\rm LM}(\vec{r}',\omega_0) \quad . \tag{2}$$

The Raman radiation $E_R(\vec{r},\omega)$ at the observer coordinate $\vec{r}$ is given by

$$E_R(\vec{r},\omega) = E_{\rm dip}(\vec{r},\omega) + E_{\rm sc}(r,\omega) \quad . \tag{3}$$

$E_{\rm dip}(\vec{r},\omega)$ is the field of the oscillating dipole $\vec{p}(\vec{r}',\omega)$ in the absence of the particle and $E_{\rm sc}(\vec{r},\omega)$ is a secondary or scattered field that must be computed by solving the appropriate boundary-value problem at the Raman frequency.

The result for a distribution of adsorbed molecules is obtained by superposition of either the Raman scattered electric fields or the power associated with each molecule, depending upon whether the emission is coherent or incoherent. The solution contains complete information about the amplitude, phase, and polarization of the inelastically scattered fields at any location for molecules at any positions outside of or at the surface of a spherical particle which may have any size or optical constants.

The details of the analysis and computed results are presented in Ref. 5. These may be stated suc-

 ©1981 The American Physical Society

cinctly. Raman scattering by molecules adsorbed at the surface of a metal sphere is enhanced by about 10^6 only if both the radius of the sphere is much less than the wavelengths ($a < 0.02\lambda$) and the relative refractive index at either the exciting or the Raman wavelength approaches $\sqrt{2}i$. This is the condition for resonant excitation of a dipolar surface plasmon. For a typical Raman shift of a molecule adsorbed on a 5-nm-radius silver particle dispersed in water there is an enhancement of $\sim 10^6$ which is sharply peaked at a 382-nm excitation wavelength. As the particle size becomes comparable to the wavelength, the enhancement is smaller but still appreciable as higher-order surface plasmons are excited. For 50 nm particles the enhancement of $\sim 10^3$ to 10^4 is broadly distributed over the visible wavelengths with a flat maximum at about 500 nm. The enhancement falls off steeply with distance of the molecule from the surface. The angular pattern of the signal strength and polarization also depends upon particle size and optical constants.

The dependence of the enhancement upon the excitation wavelength has been a central feature of SERS which experimentalists have attempted to describe and with which theorists have had to contend.[1–4,7] There has been little concordance among these various results and, more particularly, we have been concerned with the discrepancy between the monotonic increase of enhancement with wavelength which we have measured for citrate adsorbed on 21-nm-radius silver particles and our theoretical prediction that the strong enhancement should be peaked narrowly about 400 nm.

A clue to the possible resolution of this discrepancy is the suggestion by McCall, Platzman, and Wolff[8] that the surface-plasmon resonance condition varies if one changes from an isolated sphere to other geometries so that the dependence of the net Raman enhancement upon the wavelength might be obtained by an appropriate distribution of resonant frequencies, i.e., an appropriate distribution of particle geometries or arrangements. This notion was pursued in much greater detail at about the same time by Gersten and Nitzan,[9] who solved the electrostatic model for a prolate hemispheroidal metallic boss protruding from an infinitely conducting plane. The dimensions of the boss are presumed to be sufficiently small so that the electrostatic approximation could be utilized, i.e., the solution of Laplace's equation with standard electrostatic boundary conditions on the surface. A further simplification was achieved by assuming that the incident light beam propagates parallel to the symmetry axis of the boss and that the Raman active molecule is located on this axis at some distance from the spheroid on the illuminated side with the molecular dipole oriented parallel to the axis. The surface-plasmon resonance frequencies and hence the excitation spectrum of SERS depend on the shape of the boss, a finding which is consistent with the apparently conflicting results obtained for the frequency dependence of SERS, since differently prepared surfaces would be characterized by different surface irregularities. Gersten and Nitzan also present analytical results for an isolated full spheroid subject to the same simplifications and Adrian[10] has provided a calculation for this model showing how the SERS factor varies with eccentricity for a particular excitation and Raman frequency.

In this paper we relax the earlier imposed restrictions for an isolated spheroid in the electrostatic limit so the spheroid may be oriented in any manner with respect to the incident beam and the molecule may be located at any position outside of or on the surface of the spheroid. We treat both prolate and oblate spheroids. Detailed numerical results are provided for a spheroid which is randomly oriented with respect to the incident beam and is covered with a monolayer of dipoles having their axes oriented perpendicular to the spheroidal surface. Enhancements are expressed with regard to randomly oriented isolated molecules having Raman polarizabilities identical to those of the adsorbed molecules. The model is articulated in Sec. II. Numerical results of SERS and discussion are presented in Sec. III for Ag, Au, and Cu along with calculations of the extinction cross sections for these systems. Section IV comprises a summary of the conclusions.

II. MODEL

We now proceed to calculate the Raman scattering due to a molecule located at or near the outer surface of a randomly oriented prolate (oblate) spheroid. The two coordinate systems needed are shown in Fig. 1. The xyz coordinates are fixed so that the z axis is parallel to the direction of incidence whereas the $x'y'z'$ coordinates are fixed on the spheroid with the z' axis parallel to the axis of symmetry. The orientation of the spheroid is defined by two angles: θ_p which is the angle between the z' and z axes, and ϕ_p which is the angle between the x axis and the projection of the z' axis on the xy plane.

A vector $\vec{A}$ in the xyz coordinates can be transformed into the $x'y'z'$ coordinates using the transformation $[T]$,

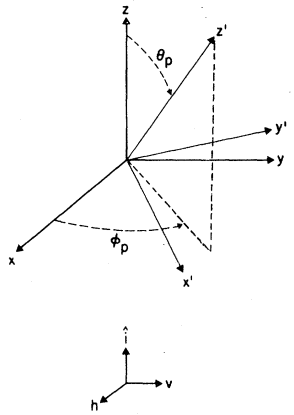

FIG. 1. Coordinate axes. Incident radiation propagates in $+z$ direction. Symmetry axis of spheroid parallel to z'.

$$\vec{A}' = [T]\vec{A} \ ,$$

where

$$[T] = \begin{bmatrix} \cos\theta_p \cos\phi_p & \cos\theta_p \sin\phi_p & -\sin\theta_p \\ -\sin\phi_p & \cos\phi_p & 0 \\ \sin\theta_p \cos\phi_p & \sin\theta_p \sin\phi_p & \cos\theta_p \end{bmatrix} . \quad (4)$$

The inverse transformation from the $x'y'z'$ coordinates to the xyz coordinates can be carried out by

$$\vec{A} = [T]^{-1}\vec{A}' \ ,$$

where $[T]^{-1} = [T]^{\dagger}$ equals the transpose of $[T]$.

Consider a plane wave incident along the z axis, and choose the xz plane as the scattering plane. The polarization of the incident wave is defined by

$$\vec{E}_0 = \begin{cases} E_h\hat{x}; & \text{horizontally polarized} \\ E_v\hat{y}; & \text{vertically polarized} \end{cases} . \quad (5)$$

In the $x'y'z'$ coordinates the incident field $\vec{E}_0'$ is given by

$$\vec{E}_0' = \begin{bmatrix} E_{0x}' \\ E_{0y}' \\ E_{0z}' \end{bmatrix} = [T]\vec{E}_0 \ . \quad (6)$$

The Raman scattering due to a molecule located outside a spheroid is first evaluated in the $x'y'z'$ coordinates. The same model used in the spherical case[5] is utilized here also. We start with the evaluation of the primary field $\vec{E}_p(\omega_0)$, which is the sum of the incident and scattered fields, at the location of the molecule. Then the dipole moment $\vec{p}_M(\omega)$ of an electric dipole induced at the location of the molecule is calculated according to Eq. (1). Finally, the Raman scattered field $E_R(\vec{r},\omega)$ [see Eq. (3)], which is the field of the dipole at the location of the molecule plus the scattered field at the shifted frequency ω due to the presence of the spheroid, is evaluated at a given scattering angle θ_s.

Prolate (oblate) spheroidal coordinates η, ϵ, and ϕ are used in the calculation instead of rectangular coordinates. The relation between η,ϵ,ϕ and x',y',z' are given as follows:

$$\begin{aligned} x' &= f[(\eta^2 \mp 1)(1-\epsilon^2)]^{1/2}\cos\phi \ , \\ y' &= f[(\eta^2 \mp 1)(1-\epsilon^2)]^{1/2}\sin\phi \ , \\ z' &= f\epsilon\eta \ , \end{aligned} \quad (7)$$

where $f = |a^2 - b^2|^{1/2}$. The minus and plus signs used here and later in this section are for the prolate and oblate spheroidal coordinates, respectively. The parameters a and b are one half of the distance along the axis of symmetry and either of the two equal axes, respectively, within a spheroidal surface for a given η.

Because the spheroids selected in this paper are sufficiently small compared to the incident wavelength, the calculation of $\vec{E}_p(\omega_0)$ is the same as the calculation of the electric field outside a spheroid in a uniform external electric field.[11] The primary field can then be given by

$$\begin{aligned} \vec{E}_p = {} & \hat{\eta}\left[\frac{\eta^2 \mp 1}{\eta^2 \mp \epsilon^2}\right]^{1/2} (P_1^1(\epsilon)\{[P_1^1(\eta)]' - g_{12}[Q_1^1(\eta)]\}(E_{0x}'\cos\phi + E_{0y}'\sin\phi) + E_{0z}'\epsilon\{1 - g_{12}[Q_1^1(\eta)]'\}) \\ & + \hat{\epsilon}\left[\frac{\eta^2 \mp 1}{\eta^2 \mp \epsilon^2}\right]^{1/2} \{[P_1^1(\epsilon)]'[P_1^1(\eta) - g_{12}Q_1^1(\eta)][E_{0x}'\cos\phi + E_{0y}'\sin\phi] + E_{0z}'[\eta - g_{11}Q_1(\eta)]\} \\ & + \hat{\phi}[(\eta^2 \mp 1)(1-\epsilon^2)]^{1/2}\{P_1^1(\epsilon)[P_1^1(\eta) - g_{12}Q_1^1(\eta)][E_{0y}'\cos\phi - E_{0x}'\sin\phi]\} \ , \end{aligned} \quad (8)$$

where $\hat{\eta}$, $\hat{\epsilon}$, and $\hat{\phi}$ are the unit vectors along the axes of the spheroidal coordinates. P_n^m and Q_n^m are the associated Legendre polynomials of the first and second kind, respectively. The primes associated with P_n^m and Q_n^m in Eq. (8) represent the derivatives with respect to the argument, and g_{11} and g_{12} are given by

$$g_{11}=\frac{\eta_0(m_0^2-1)}{m_0^2Q_1(\eta_0)-\eta_0Q_1^1(\eta_0)} ,$$
$$g_{12}=\frac{\eta_0(m_0^2-1)}{(m_0^2-1)Q_1^1(\eta_0)[P_1^1(\eta_0)]'-2/(\eta_0^2-1)} , \tag{9}$$

where m_0 is the refractive index of the spheroid relative to the medium, and η_0 is the value of the spheroidal coordinate which defines the surface of the spheroid under consideration. Note that the argument η in P_n^m and Q_n^m is for prolate spheroidal coordinates. If oblate spheroidal coordinates are used, η in P_n^m and Q_n^m should be replaced by $i\eta$. $P_n^m(i\eta)$ and $Q_n^m(i\eta)$ are given in Refs. 11 and 12.

If we let $\underline{\alpha}_m=\hat{\eta}\hat{\eta}$, i.e., the dipole unit polarizability induced at the location of the molecule is normal to the surface of the spheroid, the dipole moment of the induced dipole for a molecule located at an arbitrary position near or on the surface $(\eta_m,\epsilon_m,\phi_m)$ can be shown to be given by

$$\vec{p}_M=\hat{\eta}\left[R_{12}\left[\frac{(\eta_m^2\mp1)(1-\epsilon_m^2)}{\eta_m^2\mp\epsilon_m^2}\right]^{1/2}(E'_{0x}\cos\phi_m+E'_{0y}\sin\phi_m)+E'_{0z}R_{11}\epsilon_m\left[\frac{\eta_m^2\mp1}{\eta_m^2\mp\epsilon_m^2}\right]^{1/2}\right] , \tag{10}$$

where

$$R_{12}=\frac{\eta_m}{(\eta_m^2\mp1)^{1/2}}-g_{12}[Q_1^1(\eta_m)]' ,$$
$$R_{11}=1-g_{11}[Q_1^1(\eta_m)]' , \tag{11}$$

where $Q_1^1(\eta_m)$ is replaced by $Q_1^1(i\eta_m)$ when the oblate spheroidal coordinates are used.

Since the Raman scattered field is calculated at a distance far from the small spheroid, it can be considered as the field due to a dipole with dipole $\vec{p}'$ located at the center of the spheroid. To evaluate $\vec{p}'$ we assume that the dipole $\vec{p}_M$ at $(\eta_m,\epsilon_m,\phi_m)$ can be approximated by two point charges, $+q$ and $-q$, located at $(\eta_m+\Delta,\epsilon_m,\phi_m)$ and $(\eta_m,\epsilon_m,\phi_m)$, respectively. The relation between the diple moment $\vec{p}_M$ and the two point charges is as follows:

$$|\vec{p}_m|=|q\Delta|_{\Delta\to0} .$$

The problem now is to solve for the potential outside the spheroid in the presence of the two point charges. The dipole moment $\vec{p}'$ is then obtained by calculating the potential at a distance far from the spheroid and comparing this with the potential due to a single electric dipole. This is because the potential calculated at a large distance is the potential due to the lowest-order calculated multipole. The potential at a distance far from a spheroid is calculated by setting $\eta\to\infty$ and also using the following replacement between the spheroidal coordinates and the spherical coordinates,

$$\eta\to\gamma/f ,$$
$$\epsilon\to\cos\theta ,$$
$$\phi\to\phi .$$

$\vec{p}'$ is then given by

$$\vec{p}'=\underline{\alpha}'\vec{E}'_0 , \tag{12}$$

where the elements of $\underline{\alpha}'$ are given as follows:

$$\alpha'_{11}=2R_{12}R_{22}\left[\frac{\eta_m^2\mp1}{\eta_m^2\mp\epsilon_m^2}\right]^{1/2}(1-\epsilon_m^2)\cos^2\phi_m ,$$
$$\alpha'_{12}=2R_{12}R_{22}\left[\frac{\eta_m^2\mp1}{\eta_m^2\mp\epsilon_m^2}\right]^{1/2}(1-\epsilon_m^2)\cos\phi_m\sin\phi_m ,$$
$$\alpha'_{13}=2R_{11}R_{22}\left[\frac{\eta_m^2\mp1}{\eta_m^2\mp\epsilon_m^2}\right]^{1/2}\epsilon_m(1-\epsilon_m^2)^{1/2}\cos\phi_m ,$$
$$\alpha'_{21}=\alpha'_{12} ,$$
$$\alpha'_{22}=2R_{12}R_{22}\left[\frac{\eta_m^2\mp1}{\eta_m^2\mp\epsilon_m^2}\right]^{1/2}(1-\epsilon_m^2)\sin^2\phi_m ,$$
$$\alpha'_{23}=2R_{11}R_{22}\left[\frac{\eta_m^2\mp1}{\eta_m^2\mp\epsilon_m^2}\right]^{1/2}\epsilon_m(1-\epsilon_m^2)^{1/2}\sin\phi_m ,$$
$$\alpha'_{31}=R_{12}R_{21}\left[\frac{\eta_m^2\mp1}{\eta_m^2\mp\epsilon_m^2}\right]^{1/2}\epsilon_m(1-\epsilon_m^2)^{1/2}\cos\phi_m ,$$
$$\alpha'_{32}=R_{12}R_{21}\left[\frac{\eta_m^2\mp1}{\eta_m^2\mp\epsilon_m^2}\right]^{1/2}\epsilon_m(1-\epsilon_m^2)^{1/2}\sin\phi_m ,$$
$$\alpha'_{33}=R_{11}R_{21}\left[\frac{\eta_m^2\mp1}{\eta_m^2\mp\epsilon_m^2}\right]^{1/2}\epsilon_m^2 , \tag{13}$$

with R_{12} and R_{11} given in Eq. (11), and R_{21},R_{22} given by

$$R_{21} = 1 - g_{21}[Q_1(\eta_m)]' \ ,$$

$$R_{22} = \frac{\eta_m}{(\eta_m^2 \mp 1)^{1/2}} - g_{22}[Q_1^1(\eta_m)]' \ . \tag{14}$$

Similar to g_{11} and g_{12} given in Eq. (10), g_{21} and g_{22} are given by

$$g_{21} = \frac{\eta_0(m^2-1)}{m^2 Q_1(\eta_0) - \eta_0[Q_1(\eta_0)]'} \ ,$$

$$g_{22} = \frac{\eta_0(m^2-1)}{(m^2-1)Q_1^1(\eta_0)[\eta_0/(\eta_0^2 \mp 1)^{1/2}] + \dfrac{2}{\eta_0^2 \mp 1}} \ . \tag{15}$$

In Eq. (15), m is the relative refractive index of the spheroid at the shifted frequency ω. As in Eqs. (8), (9), and (11), $Q_n^m(\eta)$ is replaced by $Q_n^m(i\eta)$ when the oblate spheroidal coordinates are used.

After the dipole $\vec{p}\,'$ is evaluated according to Eq. (12) the Raman scattered field $\vec{E}_R'$ in the $x'y'z'$ coordinates is calculated[13] by

$$\vec{E}_R' = \frac{e^{ikr}}{r} k^2[\vec{p}\,' - \hat{n}_s'(\hat{n}_s' \cdot \vec{p}\,')] \ , \tag{16}$$

where $\hat{n}_s'$ is a unit vector in the $x'y'z'$ coordinates along the direction of observation and k is the wave number at ω, the shifted Raman frequency. In the xyz coordinates, the Raman scattered field due to a Raman scattering molecule located at $(\eta_m,\epsilon_m,\phi_m)$ outside a spheroid is obtained by transforming $\vec{E}_{RS}'$ back to xyz coordinates

$$\vec{E}_R = [T]^{-1}\vec{E}_R'$$

or

$$\vec{E}_R = \frac{e^{ikr}}{r} k^2[T]^{-1}[\vec{p}\,' - \hat{n}_s'(\hat{n}_s' \cdot \vec{p}\,')] \ . \tag{17}$$

Since

$$\hat{n}_s = [T]^{-1}\hat{n}_s' \ ,$$

$$\hat{n}_s' \cdot \vec{p}\,' = \hat{n}_s \cdot [T]^{-1}\vec{p}\,' \ ,$$

Eq. (17) becomes

$$\vec{E}_R = \frac{e^{ikr}}{r} k^2(\underline{1} - \hat{n}_s\hat{n}_s)\cdot[T]^{-1}\vec{p}\,' \ , \tag{18}$$

where $\underline{1}$ is a unitary dyadic and $\hat{n}_s$ is the unit vector along the direction of observation in the xyz coordinates. In the xz plane, which is the scattering plane, $\hat{n}_s$ is given by

$$\hat{n}_s = \begin{bmatrix} \sin\theta_s \\ 0 \\ \cos\theta_s \end{bmatrix} \ , \tag{19}$$

where θ_s is the scattering angle.

Substituting Eqs. (6) and (12) into Eq. (18) gives

$$\vec{E}_R = \frac{e^{ikr}}{r} k^2(\underline{1} - \hat{n}_s\hat{n}_s)[T]^{-1}\underline{\alpha}'[T][T]^{-1}\vec{E}_i'$$

or

$$\vec{E}_R = \frac{e^{ikr}}{r} k^2(\underline{1} - \hat{n}_s\hat{n}_s)\cdot\underline{\alpha}\cdot\vec{E}_i \ , \tag{20}$$

where

$$\underline{\alpha} = [T]^{-1}\underline{\alpha}'[T] \ . \tag{21}$$

The far-field amplitude is given by

$$\vec{F}(\theta_s,\phi_s) = k^2(\underline{1} - \hat{n}_s\hat{n}_s)\cdot\underline{\alpha}\cdot\vec{E}_i \ , \tag{22}$$

and the Raman scattering intensity is proportional to

$$|\vec{F}(\theta_s,\phi_s)|^2 = k^4|(\underline{1} - \hat{n}_s\hat{n}_s)\cdot\underline{\alpha}\cdot\vec{E}_i|^2 \ . \tag{23}$$

According to Eqs. (5) and (19) with the xz plane as the scattering plane, the various polarized components, i.e., $|\vec{F}_{V_v}|^2$, $|\vec{F}_{V_h}|^2$, $|\vec{F}_{H_h}|^2$, and $|\vec{F}_{H_h}|^2$, are given by

$$\begin{aligned}
|\vec{F}_{V_v}(\theta_s)|^2 &= k^4|\alpha_{22}|^2E_v^2 \ , \\
|\vec{F}_{V_h}(\theta_s)|^2 &= k^4E_v^2[|\alpha_{12}|^2\cos^2\theta_s + |\alpha_{32}|^2\sin^2\theta_s + (\alpha_{12}\alpha_{32}^* + \alpha_{12}^*\alpha_{32})\cos\theta_s\sin\theta_s] \ , \\
|\vec{F}_{H_v}(\theta_s)|^2 &= k^4E_h^2|\alpha_{22}|^2 \ , \\
|\vec{F}_{H_h}(\theta_s)|^2 &= k^4E_h^2[|\alpha_{11}|^2\cos^2\theta_s + |\alpha_{31}|^2\sin^2\theta_s + (\alpha_{11}\alpha_{31}^* + \alpha_{11}^*\alpha_{31})\cos\theta_s\sin\theta_s] \ ,
\end{aligned} \tag{24}$$

where $\phi_s = 0$ in the xz plane and α_{ij} represents the elements of $\underline{\alpha}$. The lower case subscripts v and h denote the polarization of the incident radiation; the upper case V and H correspond to the scattered radiation [see Eq. (5)]. Thus V_h represents the polarized component of the power scattered into a particular direction whose electric vector is perpendicular to the scattering plane for incident radiation polarized parallel to this plane.

The enhancement is determined by comparison with the Raman scattering of a molecule in the absence of the spheroid. Since such a molecule is taken to be an isolated, randomly oriented dipole in the medium, the Raman scattering intensity obtained by averaging the radiation over all orientations of the dipole is directly proportional to $|\vec{F}'(\theta_s)|^2$ which for each of the polarized components is given by

$$
\begin{aligned}
|\vec{F}'_{V_v}(\theta_s)|^2 &= \frac{k^4}{5}E_v^2 \ , \\
|\vec{F}'_{H_h}(\theta_s)|^2 &= \frac{k^4}{15}E_h^2 \ , \\
|\vec{F}'_{V_h}(\theta_s)|^2 &= \frac{k^4}{15}E_v^2 \ , \\
|\vec{F}'_{H_h}(\theta_s)|^2 &= \frac{k^4}{15}(2\cos^2\theta_s + 1)E_h^2 \ .
\end{aligned}
\tag{25}
$$

The Raman scattering intensity is directly proportional to $|\vec{F}(\theta_s,\phi_s)|^2$ so that we may define an enhancement factor as follows:

$$
G_{V_v} = \frac{|\vec{F}_{V_v}(\theta_s)|^2}{|\vec{F}'_{V_v}(\theta_s)|^2}; \quad \phi_s = 0 \tag{26}
$$

with corresponding definitions for G_{H_v}, G_{V_h}, and G_{H_h}.

The formalism presented so far is for a single molecule located at an arbitrary location $(\eta_m,\epsilon_m,\phi_m)$ outside a spheroid with a fixed orientation. For a spheroid with a given orientation covered by a monolayer of molecules, the spontaneous Raman scattering is directly proportional to the incoherent superposition of $|\vec{F}(\theta_s,\phi_s)|^2$ of the molecules on the surface of the spheroid. This is obtained by numerically integrating $|\vec{F}(\theta_s,\phi_s)|^2$ over the surface

$$
|\vec{F}(\theta_s,\phi_s)|_{\mathrm{ML}} = \frac{1}{\Delta}\int_s |\vec{F}(\theta_s,\phi_s)|^2 ds \ ,
$$

where Δ is the surface area of the spheroid. It is necessary, assuming a uniform density of molecules, to divide the surface integral by the surface area in order to compare the same number of molcules on the surface as the size or shape of the spheroid changes.

Furthermore, for a randomly oriented spheroid, the average over all orientations is required. Since the information about the location of the molecules and the orientation of the spheroid is contained entirely in $\underline{\alpha}$, to average $|F(\theta_s,\phi_s)|^2_{\mathrm{ML}}$ over all orientations is equivalent to averaging the elements of $\underline{\alpha}$ in Eq. (24) over both the location of the molecules on the surface and the orientation of the spheroid. According to Eq. (21) the average of $\alpha_{ij}\alpha^*_{i'j'}$ in Eq. (24) can be written as follows:

$$
\langle \alpha_{ij}\alpha^*_{i'j'}\rangle = \sum_{lk}\sum_{l'k'}\langle \alpha'_{lk}\alpha'^*_{l'k'}T_{li}T_{kj}T_{l'i'}T_{k'j'}\rangle \ ,
$$

where α'_{lk} and $\alpha'^*_{l'k'}$ are the elements and their complex conjugates of $\underline{\alpha'}$ given in Eq. (13). It can be seen that $\alpha'_{lk}\alpha'^*_{l'k'}$ depends on the location of the molecules, and $T_{li}T_{kj}T_{l'i'}T_{k'j'}$ on the orientation of the spheroid. Therefore the evaluation of $\langle \alpha_{ij}\alpha^*_{i'j'}\rangle$ involves the average of $\alpha'_{lk}\alpha'^*_{l'k'}$ over the location of the molecules and the averages of $T_{li}T_{kj}T_{l'i'}T_{k'j'}$ over the orientation of the spheroid.

We have evaluated the average analytically and found that $\langle \alpha_{ij}\alpha^*_{i'j'}\rangle$ is zero for $i \neq i'$, $j \neq j'$, and for $i = i'$, $j = j'$ they are given by

$$
\begin{aligned}
|\alpha_{11}|^2 &= \tfrac{4}{5}|R_{12}R_{22}|^2(\eta_m \mp 1)\frac{k_1}{\Delta} \\
&\quad + \tfrac{1}{15}[4|R_{11}R_{22}|^2 + |R_{12}R_{21}|^2 + 2(R_{12}R_{22}R^*_{11}R^*_{21} + R^*_{12}R^*_{22}R_{11}R_{21} \\
&\quad + R_{11}R_{22}R^*_{12}R^*_{21} + R^*_{11}R^*_{22}R_{12}R_{21})](\eta_m^2 \mp 1)\frac{k_2}{\Delta} + \tfrac{1}{5}|R_{11}R_{21}|^2(\eta_m^2 \mp 1)\frac{k_3}{\Delta} \ , \\
\langle |\alpha_{22}|^2\rangle &= \langle |\alpha_{11}|^2\rangle;\langle |\alpha_{12}|^2\rangle = \langle |\alpha_{31}|^2\rangle = \langle |\alpha_{32}|^2\rangle = \tfrac{1}{3}\langle |\alpha_{11}|^2\rangle \ ,
\end{aligned}
\tag{27}
$$

where for the prolate spheroid,

$$\Delta = (\eta_m^2 - 1)^{1/2} + \eta_m^2 \sin^{-1}\frac{1}{n_m} \ ,$$

$$k_1 = \tfrac{3}{2}(\eta_m^2 - 1)^{1/2}(1 - \tfrac{1}{2}\eta_m^2) + (2 - 2\eta_m^2 + \tfrac{3}{4}\eta_m^4)\sin^{-1}\frac{1}{\eta_m} \ ,$$

$$k_2 = (\tfrac{3}{4}\eta_m^2 - \tfrac{1}{2})(\eta_m^2 - 1)^{1/2} + \eta_m^2(1 - \tfrac{3}{4}\eta_m^2)\sin^{-1}\frac{1}{\eta_m} \ ,$$

$$k_3 = \tfrac{3}{4}\eta_m^4 \sin^{-1}\frac{1}{\eta_m} - (\tfrac{1}{2} + \tfrac{3}{4}\eta_m^2)(\eta_m^2 - 1)^{1/2} \ ,$$

and for the oblate spheroid,

$$\Delta = (\eta_m^2 + 1)^{1/2} + \frac{\eta_m^2}{2}\ln\frac{(\eta_m^2 + 1)^{1/2} + 1}{\eta_m^2 + 1)^{1/2} - 1} \ ,$$

$$k_1 = (1 + \eta_m^2 + \tfrac{3}{8}\eta_m^4)\ln\frac{(\eta_m^2 + 1)^{1/2} + 1}{(\eta_m^2 + 1)^{1/2} - 1} - (\tfrac{3}{2} + \tfrac{3}{4}\eta_m^2)(\eta_m^2 + 1)^{1/2} \ ,$$

$$k_2 = (\tfrac{1}{2} + \tfrac{3}{4}\eta_m^2)(\eta_m^2 + 1)^{1/2} - \left[\frac{\eta_m^2}{2} + \tfrac{3}{8}\eta_m^4\right]\ln\frac{(\eta_m^2 + 1)^{1/2} + 1}{(\eta_m^2 + 1)^{1/2} - 1} \ ,$$

$$k_3 = (\tfrac{1}{2} - \tfrac{3}{4}\eta_m^2)(\eta_m^2 + 1)^{1/2} + \tfrac{3}{8}\eta_m^4 \ln\frac{(\eta_m^2 + 1)^{1/2} + 1}{(\eta_m^2 + 1)^{1/2} - 1} \ .$$

Consequently, for a randomly oriented spheroid covered with a monolayer of molecules, Eq. (24) becomes

$$\begin{aligned}
|\vec{F}_{V_v}(\theta_s)|^2 &= k^4\langle|\alpha_{11}|^2\rangle E_v^2 \ , \\
|\vec{F}_{H_v}(\theta_s)|^2 &= \frac{k^4}{3}\langle|\alpha_{11}|^2\rangle E_v^2 \ , \\
|\vec{F}_{V_h}(\theta_s)|^2 &= \frac{k^4}{3}\langle|\alpha_{11}|^2\rangle E_h^2 \ , \\
|\vec{F}_{H_v}(\theta_s)|^2 &= \frac{k^4}{3}\langle|\alpha_{11}|^2\rangle(2\cos^2\theta_s + 1)E_h^2 \ .
\end{aligned} \tag{28}$$

From Eqs. (25), (26), and (28) it can be seen that the enhancement factor for each of the polarized components is the same and given by

$$G = 5\langle|\alpha_{11}|^2\rangle \ . \tag{29}$$

III. RESULTS AND DISCUSSION

The numerical results presented in this section, based on Eq. (29), are for randomly oriented spheriods covered with a monolayer of Raman scattering molecules. Just as in the spherical case,[5] the molecules are described by an electric dipole with dipole moment oriented normal to the surface. The spheroids are taken to be sufficiently small so that the electrostatic approximation holds. The enhancement of the Raman signal compared to that of an isolated, randomly oriented dipole located in the ambient medium has been investigated by varying the axial ratio of the spheroid a_0/b_0 where a_0 is the semi-axis along the axis of symmetry (z' axis) and b_0 is the semi-axis along either of the two equal axes. The dependence of the enhancement upon excitation wavelength has also been compared with the extinction spectrum.

As indicated in Sec. II, we assume the incident wave is along the z axis and all observations are taken to occur in the xz plane. Since the calculations made in this paper are for the electrostatic limit, the differential scattering cross sections according to Eq. (24), for each of the polarized components are identical to those of an isolated, randomly oriented dipole, and hence each of the four polarized components has the same enhancement factor which is given by Eq. (29).

The Raman shift has been selected at 1010 cm^{-1} corresponding to the well-known pyridine band and, in one instance, at 1400 cm^{-1} corresponding to a prominent citrate band. Silver, gold, and copper for which dipolar surface plasmons may be excited in the visible spectrum have been chosen to illustrate the enhancement effects. Since the experiments with colloids have been carried out in aqueous systems

(hydrosols), the values, relative to water, of the vacuum refractive indices obtained by Johnson and Christy[14] have been used in the calculations.

Figure 2 depicts the enhancement of the 1010-cm^{-1} band over the excitation wavelength range 350–650 nm for randomly oriented monolayer-covered silver prolate spheroids with the axial ratios equal to 1.0, 1.5, 2.0, 2.5, and 3.0 ($a_0/b_0 = 1$ is for a sphere). The maximum enhancement increases in magnitude and shifts toward longer excitation wavelengths as the axial ratio increases. For example, for $a_0/b_0 = 1.0$, $G = 8.3 \times 10^5$ at $\lambda_0 = 382$ nm, whereas for $a_0/b_0 = 3.0$, $G = 2.8 \times 10^7$ at $\lambda_0 = 575$ nm.

An interesting aspect of each excitation curve is the two closely spaced peaks which are separated precisely by the Raman shift, in this case 1010 cm^{-1}. That this is a general feature is shown in Fig. 3 where the Raman band is now at 1400 cm^{-1} and again the larger separation of the peaks is precisely equivalent to this new frequency shift. Still another interesting aspect is that in both cases (Figs. 2 and 3) the second (longer wavelength) of each pair of peaks occurs at the same excitation wavelength for both the 1010-cm^1 and the 1400-cm^{-1} Raman shifts. Accordingly, the first peak of each pair occurs at a correspondingly lower excitation wavelength for the 1400-cm^1 Raman shift.

In order to investigate the above effects more closely, we have calculated the extinction cross sections for randomly oriented silver spheroids over the same range of wavelengths and the same axial ratios as in Figs. 2 and 3. The extinction cross section, which is the sum of the scattering and absorption cross sections, was given by Gans[15] in the small spheroid (electrostatic) limit based upon polarizabilities initially calculated by Maxwell.[16] The interaction between the incident wave and a spheroid can be described by the radiation of a lossy dipole induced at the center of the spheroid. The polarizability component along a particular axis[6] is

$$\alpha = \frac{V(m^2 - 1)}{4\pi + (m^2 - 1)P} \tag{30}$$

where V is the volume, and the depolarization factor for the polarizability along the axis of symmetry for prolate spheroids is

$$P' = 4\pi \frac{1 - e^2}{e^2} \left[\frac{1}{2e} \ln \left[\frac{1 + e}{1 - e} \right] - 1 \right] . \tag{31}$$

For oblate spheroids, it is

$$P' = \frac{4\pi}{e^2} \left[1 - \left[\frac{1 - e^2}{e^2} \right] \sin^{-1} e \right] , \tag{32}$$

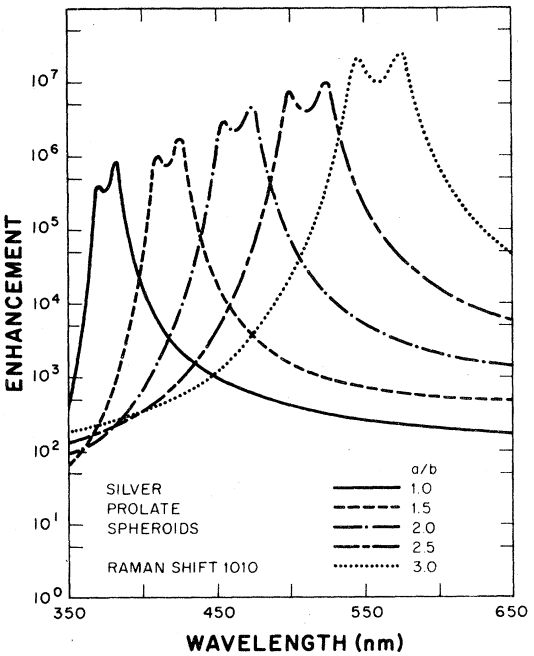

FIG. 2. Enhancement of 1010 cm^{-1} Raman line vs excitation wavelength (in vacuum) for a monolayer adsorbed on randomly oriented silver prolate spheroids in water for various axial ratios (a_0/b_0).

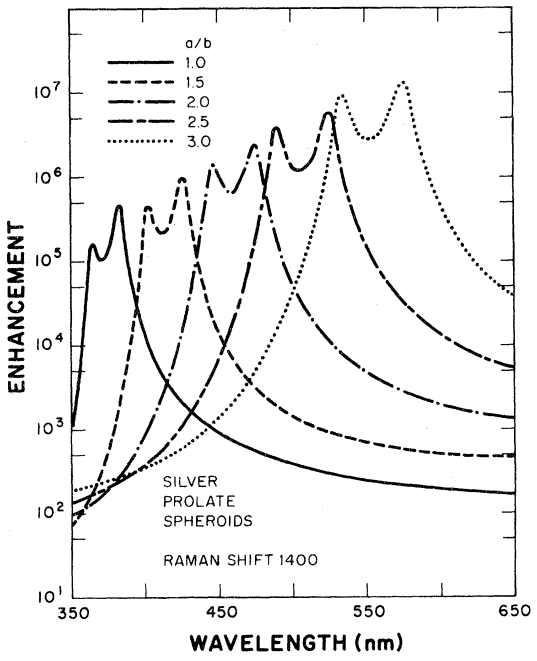

FIG. 3. Same as Fig. 2 for 1400 cm^{-1} Raman line.

where

$$e = \left[\frac{a_0^2 - b_0^2}{a_0^2}\right]^{1/2} .$$

For prolate spheroids a_0 is the axis of symmetry; for oblate spheroids b_0 is the axis of symmetry. The depolarization factor along each of the two equal axes is given by

$$P'' = (4\pi - P')/2 \ . \tag{33}$$

The extinction cross section of randomly oriented Ag prolate spheroids dispersed in water is plotted in Fig. 4 as a function of wavelength for several axial ratios. The central features of these curves are the two sharp extinction peaks for the spheroids and the single peak for the sphere. Unlike larger dielectric particles for which structures in the extinction curves arise from resonances in the various multipole moments,[6] these peaks are due to excitation of the two dipolar surface-plasmon resonances; the extinction peak at the higher wavelengths corresponds to the axis of symmetry, that at the lower wavelengths to the other two axes. It should be noted that for small particles absorption makes the predominant contribution to extinction so that high extinction implies a strong electric field within the particle. Since this field is uniform, the fields at the surface, both within and outside of the particle, are each correspondingly high. Therefore high extinction implies high local fields for stimulation of the Raman process.

Comparison of Figs. 2 and 3 with Fig. 4 shows that the second peak in each of the curves in Figs. 2 and 3 is located at the same excitation wavelength as the wavelength for maximum extinction in Fig. 4. The physical origin of the double peak is now apparent if one recalls that in our model the Raman field is the product of two processes, viz., (1) stimulation of the molecule by the local field at the incident wavelength, (2) scattering of the Raman field at the shifted wavelength by the particle. Dispersion of the refractive index obviates the possibility that both wavelengths can correspond precisely to the condition for resonance of the dipolar surface plasmon. Accordingly, the second of each pair of peaks, being at the wavelength of the extinction peak, is due to stimulation of the Raman process by the strong local field which in turn corresponds to the condition for resonance of the dipolar surface plasmon. On the other hand, the first peak of each pair is stimulated by an incident wavelength which is off resonance, but now the Raman-shifted signal is enhanced because it interacts (scatters) with the particle at the resonance condition.

Figures 5 and 6 illustrate enhancement and extinction results comparable to those in Figs. 2 and 4 but for oblate spheroids. The qualitative features

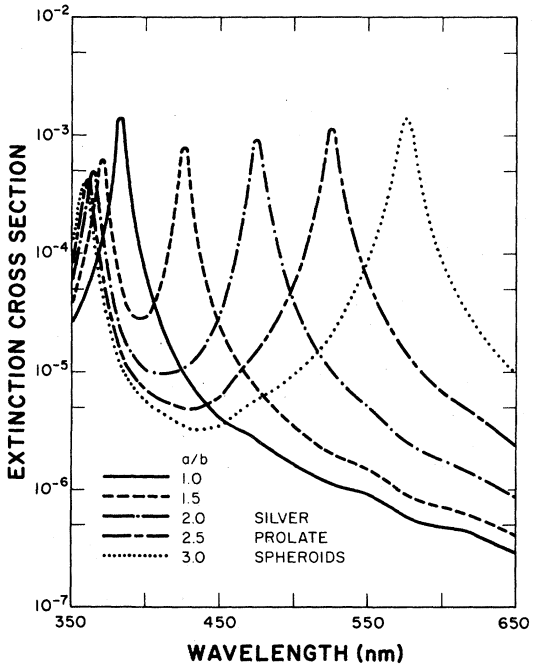

FIG. 4. Extinction cross section for small silver prolate spheroids in water for various axial ratios.

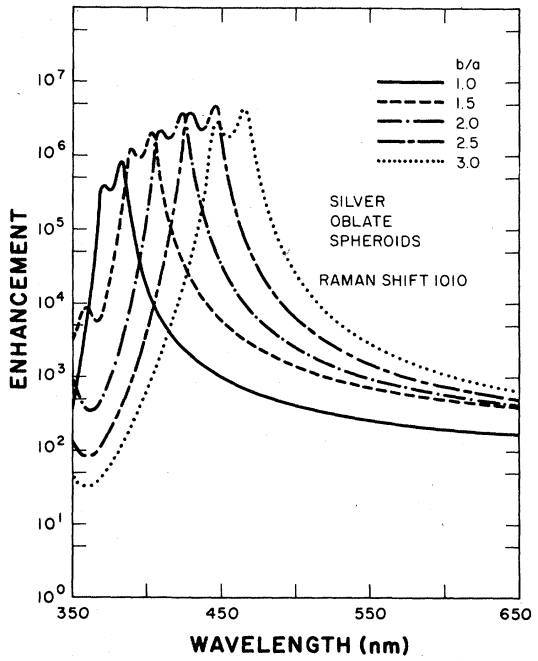

FIG. 5. Same as Fig. 2 for oblate spheroids.

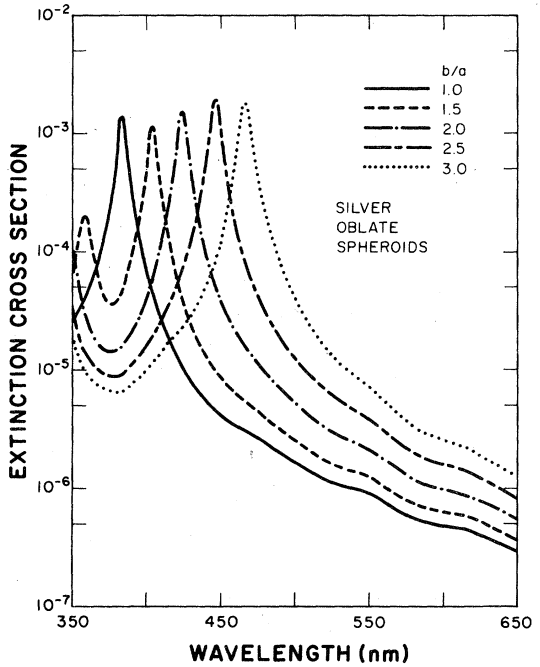

FIG. 6. Same as Fig. 4 for oblate spheroids.

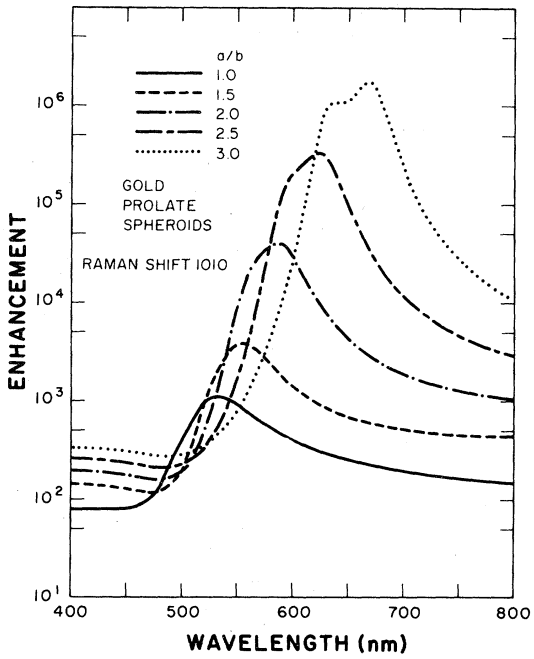

FIG. 7. Same as Fig. 2 for gold.

are the same; i.e., the double peaks whose separation equals the Raman shift move to longer wavelengths with increasing eccentricity of the oblate spheroids; the longer-wavelength peak of each doublet occurs at an excitation wavelength at which the extinction exhibits a sharp maximum. However, the shift to longer wavelengths with increasing eccentricity is not as great for these oblate spheroids as for the prolate spheroids.

Similar enhancement calculations for gold prolate spheroids are shown in Fig. 7 except that the excitation wavelength is now taken from 400 to 800 nm. The effect of increasing eccentricity is striking. Not only does the maximum enhancement shift to longer excitation wavelengths as for silver, but in this case the enhancement increases sharply from $\sim 10^3$ to $\sim 2 \times 10^6$ as a_0/b_0 changes from 1.0 to 3.0. The extinction, shown in Fig. 8, exhibits a corresponding pattern. The extinction maxima occur at the same wavelengths as the enhancement maxima with the peak extinction cross sections rising nearly an order of magnitude as the particle is extended from a sphere to a prolate spheroid with axial ratio 3.0. Another aspect is that only the most eccentric spheroid shows a double peak. This is because of the broader extinction curves so that either excitation into the extinction peak or Raman scattering into this peak does not result in a significantly greater Raman enhancement than when either of these processes occurs at neighboring wavelengths. The emergence of the double peak for axial ratio 3.0 results from the narrowing of the extinction curve with increasing axial ratio.

Figures 9 and 10 give corresponding results for Cu. The qualitative features are similar to those for gold, except that in this case the enhancement and

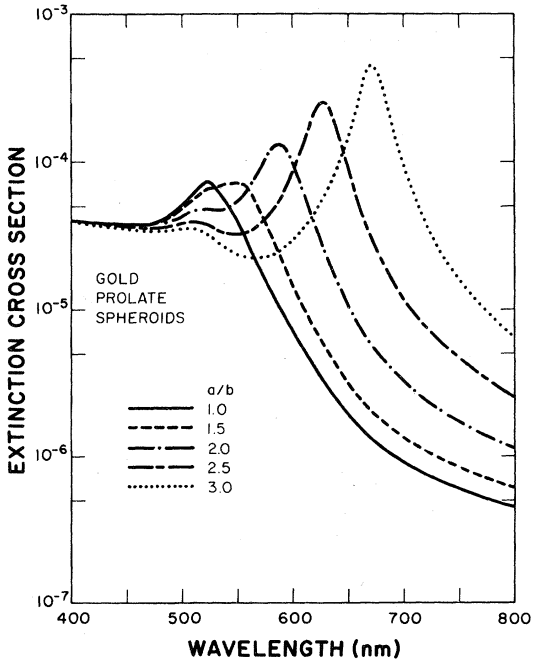

FIG. 8. Same as Fig. 4 for gold.

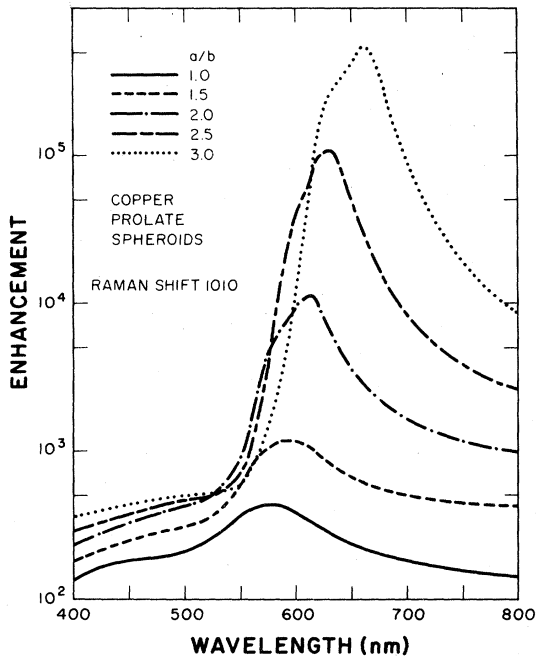

FIG. 9. Same as Fig. 2 for copper.

extinction maxima are not displaced to longer wavelengths as sharply as gold. The double peak which Au exhibits at axial ratio 3.0 fails to emerge with Cu, a result which is consistent with the somewhat broader extinction curve for Cu. The corresponding peak enhancements for Cu are less than those for gold which is also consistent with the lower corresponding values of the extinction cross section.

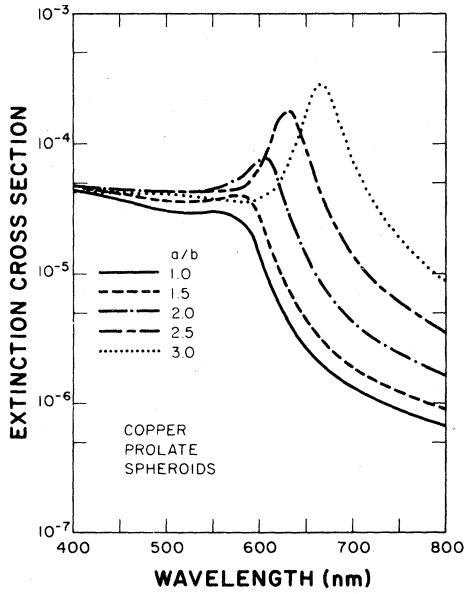

FIG. 10. Same as Fig. 4 for copper.

Each of the longer-wavelength extinction maxima for Ag in Figs. 4 and 6 as well as the extinction maxima for Au and Cu in Figs. 8 and 10 correspond to resonant excitation along the axis of symmetry. There are additional extinction maxima for Au and Cu at wavelengths less than 400 nm and, just as for Ag, these correspond to excitations along the equal axes. One would expect corresponding enhanced Raman scattering for excitation or for Raman emission at these wavelengths.

We conclude with a warning lest there be a tendency among some to generalize the results of this study beyond the range of its validity, namely, for particles larger than those for which the electrostatic limit applies. That limit can be definitively prescribed only for spheres for which the general electrodynamic solution has been obtained.[5] For silver spheres it is $a < 0.02\lambda$; this limit may differ somewhat for markedly different optical constants. For spheroids one may presume 0.02λ to be the limit on the longer dimension although a firm conclusion must await extension of the present model to spheroids of arbitrary size.

The generalizations against which we warn are illustrated in Fig. 11 for a 5-nm Ag sphere in water where the peak in the enhancement corresponds precisely to the peaks in the absorption, scattering, and extinction curves. Excitation is into the dipolar

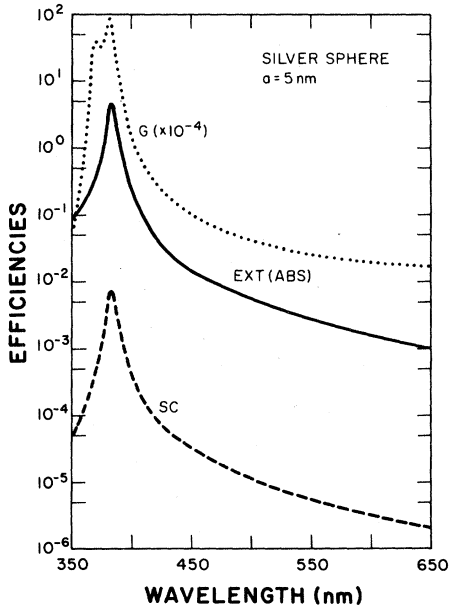

FIG. 11. Comparison of vacuum wavelength dependence of extinction, scattering, and absorption cross sections with dependence of enhancement of the 1010 cm^{-1} Raman shift of an adsorbed monolayer for 5 nm silver spheres in water.

surface-plasmon resonance or the Raman emission is into this resonance. With larger particles one is dealing with a superposition of multipolar fields[6] rather than with a dipolar field (or two or three dipolar fields corresponding to the spheroid or ellipsoidal polarizabilities). The extinction and Raman enhancement are not linked in a simple linear fashion. The absorption cross section is related to the distribution of lossy sinks throughout the particle which in turn is determined by what may be a very complicated distribution of the electric field.[17] The scattering cross section is the spatial average of the squared modulus of the field in the radiation zone. The Raman signal, on the other hand, arises in two steps. The molecule is stimulated by a local field comprised of the near field elastically scattered by the particle coherently added to the incident field; then the observer views the superposition of the dipolar field of the Raman molecule also coherently added to a field elastically scattered by the particle at the Raman wavelength.

Figures 12 and 13 illustrate the various cross sections for 50 and 500-nm-radius Ag spheres, respectively. The SERS excitation spectra had been presented earlier.[5] The absorption, scattering, and extinction spectra were calculated with the Lorenz-Mie equations.[6] In Fig. 12, for which the spherical radius is $a = 50$ nm, there is a broad peak in the extinction curve in the region of 500 nm wavelength, the enhancement follows a quite different pattern at lower wavelengths. The sharp extinction peak at 380 nm does not translate into a corresponding large enhancement.

Figure 13 compares the extinction, scattering, and absorption spectra for a 500 nm particle, with the SERS excitation spectra. The disparity between the SERS and the Lorenz-Mie cross sections is even more apparent for this larger particle. The extrema of the latter occur at precisely the same wavelengths even though the logarithmic plot does appear to dampen the amplitudes of the oscillations in the extinction and scattering curves compared to the absorption curves. However, the peaks in the SERS excitation curve appear to be quite unrelated. This is apparently due to the fact that the local field which excites the process is the superposition of the elastic scattered near field plus the incident field, and also that the scattering process at the Raman-shifted wavelength is no longer simply related to that at the incident wavelength.

IV. CONCLUSION

Equations have been derived for Raman scattering by molecules located outside of or at the surface of a prolate and oblate spheroids sufficiently small that the electrostatic approximation may be applied. Raman scattering consists of two steps: (1) stimulation of the Raman process by a local field comprised of

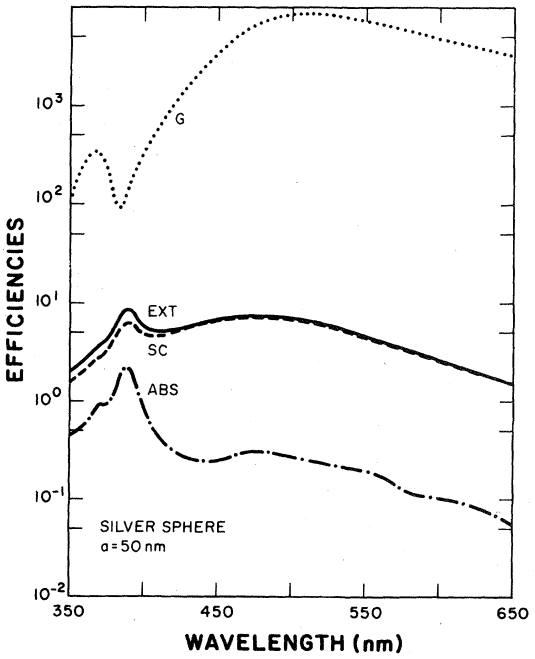

FIG. 12. Same as Fig. 11 for 50 nm spheres.

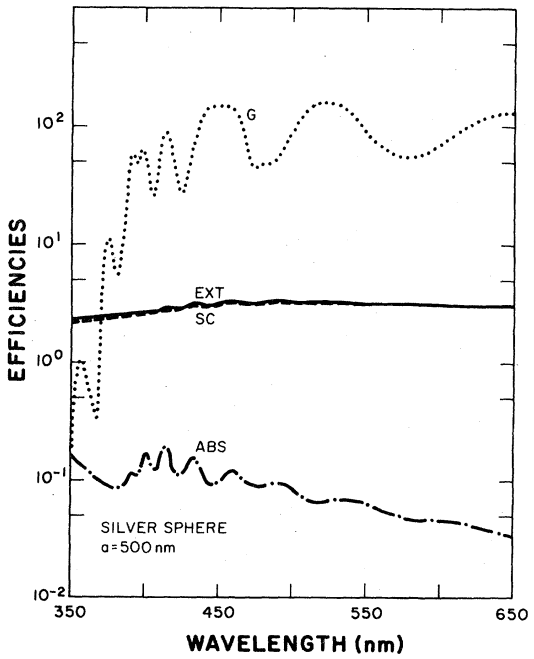

FIG. 13. Same as Fig. 11 for 500 nm spheres.

the incident and scattered field at the incident wavelength, (2) interaction (scattering) of the Raman radiation by the particle at the shifted frequency with the particle. The results are expressed as differential scattering cross sections of each of the four polarized components of the radiation [Eq. (24)]. The spheroidal particle may be arbitrarily oriented with respect to the arbitrarily polarized incident beam. The Raman scattering molecule, treated as a classical electric dipole, may be located at any position outside of or at the surface of the particle, and it may have any orientation with regard to the surface. The differential scattering cross sections [Eq. (28)] and the enhancement factor compared to a randomly oriented isolated molecule [Eq. (29)] are given for a monolayer of dipolar molecules oriented perpendicular to the surface of a spheroid, which in turn is randomly oriented with respect to the incident beam.

Calculations of the enhancement factor defined above [Eq. (29)] are presented over the visible spectrum for Ag, Au, and Cu hydrosols and these are compared with the corresponding extinction spectra. In each case very large enhancements occur over a narrow range of wavelengths. These maximum enhancements shift to longer wavelengths as the axial ratio increases and in the case of Au and Cu there is a striking increase in the magnitude of the enhancement with increasing eccentricity. There is a corresponding increase in extinction at the corresponding wavelengths. In each case the excitation wavelengths of the region of large enhancement correspond to the wavelengths for which there is a maximum in the extinction spectrum. For Ag the enhancement maximum is bimodal. One of these peaks corresponds to excitation of the Raman process at the wavelength of maximum extinction, i.e., at the condition for resonance of the dipolar surface plasmon. The other peak corresponds to excitation at a sufficiently lower wavelength so that Raman emission is at the dipolar surface plasmon resonance. The dual peaks for Ag are no longer apparent for Au and Cu and this is related to the broader extinction maxima for these substances.

The simple relations described above are no longer obtained when the particles are sufficiently large so that the electrostatic approximation no longer applies. In any case it is quite clear that both the qualitative and quantitative features of SERS as described by this electrodynamic model are quite sensitive to particle morphology. Cooperative effects such as those due to arrays of interacting particles[1] as well as those due to varying surface coverage[18] with consequent interactions of any of the adsorbed molecules must also be considered in any complete electrodynamic model. It seems reasonable to expect comparable dependence upon the particular kinds of "roughnesses" encountered on macroscopic surfaces so that the admonitions expressed by McCall, Platzman, and Wolff[8] and by Gersten and Nitzan[9] should be heeded; different experimental systems may show very different effects.

It should also be stressed that we have only considered the effects of the classical electromagnetic fields upon the Raman process and have assumed that the molecular polarizability $\underline{\alpha}_m$ in Eq. (1) is the same for the adsorbed as for the isolated molecules. A more complete theory must of course deal with this important and very interesting effect, viz., the specific interaction between the molecules and the metal.

ACKNOWLEDGMENT

This work was supported in part by Army Research Office Grant No. DAAG-29-79-C-0059 and National Science Foundation Grant No. CHE-8011444.

[1] M. Moskovits, J. Chem. Phys. 69, 4159 (1978).
[2] J. A. Creighton, C. G. Blatchford, and M. G. Albrecht, J. Chem. Soc. Faraday Trans. 2 75, 790 (1979).
[3] H. Wetzel and H. Gerischer, Chem. Phys. Lett. 76, 460 (1980); M. E. Lippitsch, *ibid.* 74, 125 (1980); K. V. Von Raben and R. K. Chang, *ibid.* 79, 465 (1981).
[4] M. Kerker, O. Siiman, L. A. Bumm, and D. -S. Wang, Appl. Opt. 19, 3253 (1980).
[5] M. Kerker, D. -S. Wang, and H. Chew, Appl. Opt. 19, 3373 (1980); see *ibid.* 19, 4159 (1980) for reprinted version in which numerous printer's errors have been corrected; also D. -S. Wang, M. Kerker, and H. Chew, Appl. Opt. 19, 2315 (1980).
[6] M. Kerker, *The Scattering of Light and Other Electromagnetic Radiation* (Academic, New York, 1969).
[7] D. L. Jeanmaire and R. P. van Duyne, J. Electroanal. Chem. 84, 1 (1977); J. A. Creighton, M. G. Albrecht, R. E. Hester, and J. D. Mathew, Chem. Phys. Lett. 55, 55 (1978); B. Pettinger, U. Wenning, and D. M. Kolb, Ber. Bunsenges. Phys. Chem. 82, 1326 (1978); M. Moskovits, Solid State Commun. 32, 59 (1979); W. H. Webber and G. W. Ford, Bull. Am. Phys. Soc. 25, 424 (1979); M. Moskovits and D. P. Dilella,

Chem. Phys. Lett. 73, 500 (1980); J. A. Creighton, C. G. Blatchford, and J. R. Campbell, *Proceedings of the Seventh International Conference on Raman Spectroscopy,* edited by W. F. Murphy (North-Holland, Amsterdam, 1980), p. 412; W. Krasser, *ibid.,* p. 420; B. Pettinger, *ibid.,* p. 412.

[8]S. L. McCall, P. M. Platzman, and P. A. Wolff, Phys. Lett. 77A, 381 (1980).

[9]J. Gersten and A. Nitzan, J. Chem. Phys. 73, 3023 (1980).

[10]F. J. Adrian, Chem. Phys. Lett. 78, 45 (1981).

[11]W. R. Smythe, *Static and Dynamic Electricity* (McGraw-Hill, New York, 1950).

[12]*Handbook of Mathematical Functions,* U. S. Natl. Bur. Stand. (Appl. Math. Ser. No. 55), edited by M. Abramowitz and I. A. Stegun (U. S. GPO, Washington, D. C., 1964).

[13]J. D. Jackson, *Classical Electrodynamics* (Wiley, New York, 1975).

[14]P. B. Johnson and R. W. Christy, Phys. Rev. B 6, 4370 (1972).

[15]R. Gans, Ann. Phys. 37, 881 (1912).

[16]J. C. Maxwell, *A Treatise on Electricity and Magnetism* (Oxford University Press, Oxford, 1873), Vol. II; 3rd ed. (Oxford University Press, Oxford, 1892), pp. 66–70.

[17]P. W. Dusel, M. Kerker, and D. D. Cooke, J. Opt. Soc. Am. 69, 55 (1979).

[18]G. L. Easely, Phys. Lett. 81A, 193 (1981).